Preprint Cambridge Centre for Computational Chemical Engineering ISSN 1473 – 4273

The suitability of particle models in capturing aggregate structure and polydispersity

William J. Menz, Markus Kraft [1]

released: December 12, 2012

[1] Department of Chemical Engineering
and Biotechnology
University of Cambridge
New Museums Site
Pembroke Street
Cambridge, CB2 3RA
United Kingdom
E-mail: mk306@cam.ac.uk

Preprint No. 123

Keywords: population balance, particle model, coagulation, sintering, polydispersity

Edited by
Computational Modelling Group
Department of Chemical Engineering and Biotechnology
University of Cambridge
New Museums Site
Pembroke Street
Cambridge CB2 3RA
United Kingdom

Fax: + 44 (0)1223 334796
E-Mail: c4e@cam.ac.uk
World Wide Web: http://como.cheng.cam.ac.uk/

Abstract

This work presents the mathematical formulation of particle models commonly used in aerosol dynamics of nanoparticles. A detailed numerical study is conducted in order to understand under which conditions these models differ. The silica model of Shekar et al. (2012, *J. Aerosol Sci.* **44** 83–98) and silicon model of Menz et al. (2013, *Combustion & Flame*, accepted for publication) model taken from the literature are analysed using three different particle models, demonstrating that substantial errors can be incurred when using a particle model inappropriate for a particular modelling application. It is concluded that the suitability of a particular particle model for a modelling purpose is dependent on the characteristic sintering and coagulation timescales of the system. The influence of particle rounding due to heterogeneous surface growth remains to be quantified.

Contents

1 Introduction

Population balance modelling is typically applied in order to model the aerosol synthesis of nanoparticles [19, 41, 45]. Depending on how the population balance equations are solved, different assumptions are made about the nature of the particles to simplify the these equations' solutions [45]. The level of detail to which the particles are described is defined as a particle model.

The type of particle model used depends on how the population balance equation is solved and the target modelling system. Three main categories of solution methodology are employed. The 'method of moments' [8, 9] describes the evolution of a population of particles by the moments of the distribution. It is typically fast, however the particle size distribution (PSD) can not be resolved from the results of such calculations. The sectional methods split the distribution of particle properties into sections [14], allowing some resolution of PSD. These methods are often more computationally expensive [45] than the moments method and can only be extended to multiple internal dimensions with great difficulties [12].

An alternative is to use stochastic methods [3, 5, 30, 31]: these approximate the real particles with a collection of 'computational particles'. The computational particles may interact with each other through a series of stochastic jump processes which define how the particles change with time. These methods have been applied to a variety of systems [5, 6, 22, 33, 34, 38]. However, the main disadvantage of stochastic methods is that it is difficult to include spatial inhomogeneity [29, 31].

In early modelling attempts, particles were treated as spheres which would coalesce into larger spheres upon collision with other particles; for example, see Frenklach and Harris [9]. This corresponds to the spherical particle model; which is a one-dimensional model tracking only the volume or some number of chemical elements in a particle.

However, not all nanoparticles are spherical [28, 36, 40]. It is very common to obtain aggregates (chemically bound collections of particles) and agglomerates (physically bound particles) [7], especially where particle growth occurs by coagulation or sintering. The surface-volume particle model extended from the basic spherical model, by tracking the volume and total surface area of a particle [20, 45]. Another 2D model providing similar information tracked the number of aggregates and number of primary particles [27]. Such knowledge provides a basic understanding of aggregate structure of particles.

The surface-volume model is limited in the respect that it assumes that primary particles are monodisperse. Further, it has been identified that typical expressions used to calculate the primary particle size are not ideal [43]. Heine and Pratsinis [12] developed a sectional model to address this issue, where the polydispersity of primary particles was incorporated in a sectional model. Balancing the population of primary particles over all aggregate particles enabled the effects of simultaneous coagulation and sintering to be captured.

Even more detailed particle models have been utilised. Sander et al. [33] presented a 'binary-tree' particle model as part of a stochastic population balance. It incorporated the full aggregate structure of soot particles, allowing for resolution of individual primary particles and their connection to other primary particles in an aggregate. This model has been extended to silica [23, 38, 39] and silicon [22, 24].

Despite these advances in modelling the structure and morphology, many studies still use basic spherical or surface-volume particle models [1, 11, 18]. This work investigates the conditions under which use of these models is appropriate; and where their use could represent a significant over-simplification. This is accomplished with a generic stochastic population balance solver [5, 10, 25, 30] which has been mathematically described and numerically investigated elsewhere [22, 33, 38].

The structure of the present work is as follows. Section 2 presents the mathematical description of the particle models and how their derived properties (e.g. particle collision diameter) are calculated. Sections 3 and 4 discuss some case studies and compares model predictions for a range of test cases; and the paper is concluded with suggestions for further research in Section 5.

2 Models

2.1 Type-space

This work uses a 'generic' multicomponent description of the primary particles' chemical composition; that is,

$$p = p\left(\eta_1, \eta_2, \ldots, \eta_n\right) \ , \tag{1}$$

where p will contain η_i chemical components (e.g. number of carbon atoms). A particle P_q of index q in $N_{\max}$ computational particles will always contain at least one primary particle p. For the spherical particle model, the *type-space* is very simple:

$$P_q = P_q\left(p^{(q)}\right) \ . \tag{2}$$

Here the super-script is used to denote ownership of the primary particle $p^{(q)}$ by particle P_q. The surface-volume model (or, surf-vol model for short) was first proposed by Kruis et al. [20]. In addition to tracking the chemical composition of particles, it also includes the surface area $S^{(q)}$ as an independent variable:

$$P_q = P_q\left(p^{(q)}, S^{(q)}\right) \ . \tag{3}$$

The surface-volume model, however, assumes that primaries in a particle P_q are uniformly distributed. The ability to include polydispersity of primary particles was proposed by Sander et al. [33] in their 'binary tree' model. This model represents a particle as a binary tree of primary particles with some manner of connectivity between them:

$$P_q = P_q\left(p_1, p_2, \ldots, p_{n_q}, \mathbf{C}^{(q)}\right) \tag{4}$$

where P_q contains n_q primary particles and $\mathbf{C}$ is a lower-diagonal matrix representing the common surface area between two neighbouring primary particles. The form of this matrix is discussed in [33, 38, 39].

Table 1: *Comparison of the derived properties of the particle models.*

Property	Spherical	Surf-vol	Binary tree
type-space	$P_q\left(p^{(q)}\right)$	$P_q\left(p^{(q)}, S^{(q)}\right)$	$P_q\left(p_1, p_2, \ldots, p_{n_q}, \mathbf{C}^{(q)}\right)$
V_q	$\sum_{i=1}^{n} \frac{\eta_i M_i}{N_\mathrm{A}\rho_i}$	$\sum_{i=1}^{n} \frac{\eta_i M_i}{N_\mathrm{A}\rho_i}$	$\sum_{j=1}^{n_q} V(p_j)$
$d_{\mathrm{sph},q}$	$\sqrt[3]{\frac{6}{\pi}V_q}$	$\sqrt[3]{\frac{6}{\pi}V_q}$	$\sqrt[3]{\frac{6}{\pi}V_q}$
$S_{\mathrm{sph},q}$	$\pi d_{\mathrm{sph},q}^2$	$\pi d_{\mathrm{sph},q}^2$	$\pi d_{\mathrm{sph},q}^2$
S_q	$S_{\mathrm{sph},q}$	$S^{(q)}$	$\frac{S_{\mathrm{sph},q}}{\bar{s}_q(1-n_q^{-\frac{1}{3}})+n_q^{-\frac{1}{3}}}$
$d_{\mathrm{pri},q}$	$d_{\mathrm{sph},q}$	$\frac{6V_q}{S_q}$	-
$\overline{d_{\mathrm{pri}}}_q$	-	-	$\frac{1}{n_q}\sum_{j=1}^{n_q} d_{\mathrm{pri}}(p_j)$
n_q	1	$\frac{S_q^3}{36\pi V_q^2}$	n_q
$d_{\mathrm{col},q}$	$d_{\mathrm{sph},q}$	$\frac{1}{2}\left(d_{\mathrm{sph},q}+\sqrt{\frac{S_q}{\pi}}\right)$	$\overline{d_{\mathrm{pri}}}_q\left[\frac{S_q^3}{36\pi V_q^2}\right]^{\frac{1}{D_\mathrm{f}}}$

2.2 Derived properties

The *type-space* of the particles allows for all other properties of the particles to be determined. The volume of a primary is based on the number of chemical units η_i and bulk densities ρ_i:

$$v(p) = \sum_{i=1}^{n} \frac{\eta_i M_i}{N_\mathrm{A}\rho_i} \tag{5}$$

where M_i is the molecular weight of element i and N_A is Avogadro's number. For spherical or surface-volume particles, the volume of the particle V_q is equal to that of the primary. In the binary tree model, the volume of a particle the sum of the volume of its constituent primaries, that is,

$$V_q = V(P_q) = \sum_{j=1}^{n_q} v(p_j)\ . \tag{6}$$

The derived properties of the surface-volume model have been published in [20]. Essentially, the volume and surface area S_q of a particle are used to estimate the size of primary particles, the number of primaries and the collision diameter. These equations are summarised in Table 1. For the binary tree model, the derived properties are analogous to those used in previous studies [22, 23, 33, 38]. Of key importance is the surface area:

$$S_q = \frac{S_{\mathrm{sph},q}}{\bar{s}_q(1-n_q^{-\frac{1}{3}})+n_q^{-\frac{1}{3}}} \tag{7}$$

where $S_{\text{sph},q}$ is the equivalent spherical surface of a sphere with the same volume as the particle P_q, and $\bar{s}_q$ is the average sintering level between the primaries of the particle. The sintering level ($0 \leq s \leq 1$) of two primary particles p_j and p_k is given by [33]:

$$s(p_j, p_k) = \frac{\frac{S_{\text{sph}}(p_j, p_k)}{C_{jk}} - 2^{-\frac{1}{3}}}{1 - 2^{-\frac{1}{3}}}. \tag{8}$$

This definition implies that a spherical particle has a sintering level of 1, while two primaries in point contact (with no sintering) have a sintering level of 0. An important distinction to make between the primary particle diameter described by the surface-volume model and that of the binary tree model is that the latter is an average within the particle, while the former is an estimate based-on the surface area and volume. Thus, the average primary diameter in a binary tree particle is given by:

$$\overline{d_{\text{pri}}}_q = \frac{1}{n_q} \sum_{j=1}^{n_q} d_{\text{pri}}(p_j). \tag{9}$$

The collision diameter of a particle is given by [38]:

$$d_{\text{col},q} = \overline{d_{\text{pri}}}_q \left[\frac{S_q^3}{36\pi V_q^2} \right]^{\frac{1}{D_\text{f}}} \tag{10}$$

where d_{pri} is the D_f is the fractal dimension, assumed to be 1.8 for the present work [35]. These are summarised and compared with the derived properties of other particle models in Table 1.

2.3 Particle processes

The three particle models interact generically with several particle processes. Examples of such processes are inception (or nucleation), heterogeneous growth, coagulation and sintering. These are documented and mathematically described in detail in [22, 23]. In the present work, coagulation and sintering are the two which differ most between models so are outlined here.

The rate of coagulation is calculated using the 'transition regime coagulation kernel' (K^{tr}), which is a computationally efficient approximation to true Brownian coagulation [15, 23]. In the spherical particle model, a coagulation event will form a sphere with volume equal to the sum of the coagulating spheres' volume. This is represented by the following transformation:

$$P_q\left(p^{(q)}\right) + P_r\left(p^{(r)}\right) \rightarrow P_s\left(p^{(q)} + p^{(r)}\right) \tag{11}$$

The addition of primary particles is equivalent to taking the sum of their component vectors:

$$p^{(q)}(\eta_1^{(q)}, \ldots, \eta_n^{(q)}) + p^{(r)}(\eta_1^{(r)}, \ldots, \eta_n^{(r)}) = p^{(s)}(\eta_1^{(q)} + \eta_1^{(r)}, \ldots, \eta_n^{(q)} + \eta_n^{(r)}) \tag{12}$$

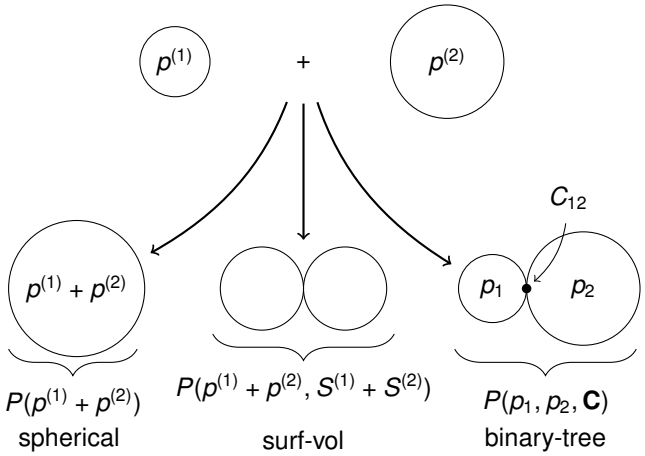

Figure 1: *An illustration of different particle models' description of coagulation events.*

A similar transformation takes place for a coagulation event in the surface-volume model, except the total surface area is also conserved:

$$P_q(p^{(q)}, S^{(q)}) + P_r(p^{(r)}, S^{(r)}) \rightarrow P_s(p^{(q)} + p^{(r)}, S^{(q)} + S^{(r)}) \,. \tag{13}$$

A coagulation event in the binary tree model will retain the primary particle information and connectivity of both coagulating particles:

$$P_q\left(p_1, \ldots, p_{n_q}, \mathbf{C}^{(q)}\right) + P_r\left(p_1, \ldots, p_{n_r}, \mathbf{C}^{(r)}\right) \rightarrow P_s\left(p_1, \ldots, p_{n_q}, p_{n_q+1}, \ldots, p_{n_q+n_s}, \mathbf{C}^{(s)}\right) \tag{14}$$

The common-surface matrix $\mathbf{C}$ is changed to reflect the structure of old particles P_q and P_s, and their new connection. The process through which this is done is described in detail by Shekar et al. [38]. The physical interpretation of Equations (11)–(14) is illustrated in Figure 1.

The three models also include quite different descriptions of sintering. For the spherical particle model, sinter effectively occurs infinitely fast, as particle coalesce upon coagulation. For the surface-volume and binary tree models, the exponential excess surface area decay formula–as popularised by Koch and Friedlander [17]–is employed. In the former of these, the surface area of the whole particle is reduced

$$\frac{\Delta S_q}{\Delta t} = -\frac{1}{\tau_{\mathrm{S}}(p^{(q)})}\left(S_q - S_{\mathrm{sph},q}\right) \tag{15}$$

where τ_{S} is the characteristic sintering time. It is an empirical function of temperature T and diameter d which is related to the time required for a two neighbouring primaries to coalesce. For the surface-volume model, it is expressed in the form

$$\tau_{\mathrm{S}}(p^{(q)}) = A_{\mathrm{S}}\, d_{\mathrm{pri},q}^{n_{\mathrm{S}}}\, T \exp\left(\frac{E_{\mathrm{S}}}{RT}\right) \tag{16}$$

where A_{S}, n_{S} and E_{S} are empirical parameters. Tracking of the connectivity of adjacent primary particles allows the binary tree model to sinter each connection individually. For

a single connection, the rate of sintering is given by

$$\frac{\Delta C_{jk}}{\Delta t} = -\frac{1}{\tau_{\mathrm{S}}(p_j, p_k)} \left(C_{jk} - S_{\mathrm{sph}}(p_j, p_k)\right) \tag{17}$$

where C_{jk} represents the element of the common-surface matrix $\mathbf{C}$ describing the common surface area of the two primaries p_j and p_k, and $S_{\mathrm{sph}}(p_j, p_k)$ is their equivalent surface area. The characteristic sintering time also takes a slightly different form to account for two primaries of a different size touching:

$$\tau_{\mathrm{S}}(p_j, p_k) = A_{\mathrm{S}} \min\left[d_{\mathrm{pri}}(p_j), d_{\mathrm{pri}}(p_k)\right]^{n_{\mathrm{S}}} T \exp\left(\frac{E_{\mathrm{S}}}{RT}\right) . \tag{18}$$

2.4 Average properties

In order to study the behaviour of a system of particles, it is useful to define some average quantities which describe the size and morphology of the particles and ensemble. In this work, the arithmetic and geometric mean of the collision and primary diameter is used. These are denoted as μ_{a} and μ_{g} respectively. For example, the geometric mean of the primary diameter is given by:

$$\mu_{\mathrm{g}}(d_{\mathrm{pri}}) = \left(\prod_{q=1}^{N(t)} d_{\mathrm{pri},q}\right)^{\frac{1}{N(t)}} \tag{19}$$

where $N(t)$ computational particles are in the ensemble at time t. Note that for the surface-volume model, $\mu_{\mathrm{g}}(d_{\mathrm{pri}})$ represents the mean of the estimated primary diameter of each particle; while in the binary tree model it represents the mean of average primary diameter of each particle. The (number-based) geometric standard deviation is also particularly useful for classifying polydispersity of particles [12]. Here, it is calculated in the context of the binary tree model for the average primary diameter as

$$\sigma_{\mathrm{g}}(\overline{d_{\mathrm{pri}}}) = \exp\left(\sqrt{\frac{1}{N(t)} \sum_{q=1}^{N(t)} \ln\left[\frac{d_{\mathrm{pri},q}}{\mu_{\mathrm{g}}(\overline{d_{\mathrm{pri}}}_q)}\right]^2}\right) \tag{20}$$

For the binary tree model, two estimates of $\sigma_{\mathrm{g}}(d_{\mathrm{pri}})$ can be made. The first involves using Equation (20) to calculate the geometric standard deviation of the average primary diameter. The second takes the arithmetic mean of the geometric standard deviation of the primary diameter in each particle:

$$\mu_{\mathrm{a}}\left[\sigma_{\mathrm{g}}(d_{\mathrm{pri}})\right] = \frac{1}{N(t)} \sum_{q=1}^{N(t)} \exp\left(\sqrt{\frac{1}{n_q} \sum_{j=1}^{n_q} \ln\left[\frac{d_{\mathrm{pri},j}}{\mu_{\mathrm{g}}(d_{\mathrm{pri}})}\right]^2}\right) \tag{21}$$

Table 2: *Parameters used in the case studies.*

Description	Symbol	Value	Ref.
Numerical parameters			
Maximum splitting timestep	Δt_s	2.5×10^{-4}	[38]
Maximum number of stochastic particles	$N_{\max}$	16,384	[23]
Number of runs	L	8	[23]
Model parameters - Silica model			
Fractal dimension	D_{f}	1.8	[35]
Sintering pre-exponential	A_{S}	1.10×10^{-16} s/m	[37]
Sintering characteristic energy	E_{S}	1.20×10^{5} K	[37]
Sintering minimum diameter	$d_{\mathrm{p,min}}$	4.4 nm	[37]
Gas-phase parameters	-	-	[37]
Model parameters - Silicon model			
Fractal dimension	D_{f}	1.56	[32]
Sintering pre-exponential	A_{S}	1.15×10^{13} s/m^4	[20]
Sintering characteristic energy	E_{S}	2.77×10^{4} K	[20]
Sintering diameter power	n_{S}	4	[20]
Gas-phase parameters	-	-	[13, 22]

3 Case studies

In order to study the structure of particles simultaneously undergoing coagulation and sintering, several properties are first defined. The characteristic coagulation time τ_{C} is given by [26, 46]

$$\tau_{\mathrm{C}} = \frac{1}{K^{\mathrm{tr}} M_0} \tag{22}$$

where K^{tr} is the transition regime coagulation kernel evaluated for the particle ensemble under study (m^3/s) and M_0 is the zeroth moment, or particle number density (1/m^3). For the cases in Sections 3.1 and 3.2, the initial characteristic coagulation time $\tau_{\mathrm{C},i}$ is used. The characteristic times are normalised by the residence time τ, yielding a dimensionless characteristic time.

3.1 Coagulation and sintering

The three models presented in the present work use very different representations of coagulation and sintering processes. To compare the models, a sample ensemble of monodisperse spherical particles of diameter d_i was generated. The initial characteristic coagulation time $\tau_{\mathrm{C},i}$ of these particles was estimated based-on their size and number density; and the sintering time τ_{S} was set to a constant value. The space of normalised coagulation time and normalised sintering time was scanned, and the resulting structures of particles analysed. Each point in this space represents a calculation for the same initialised ensemble

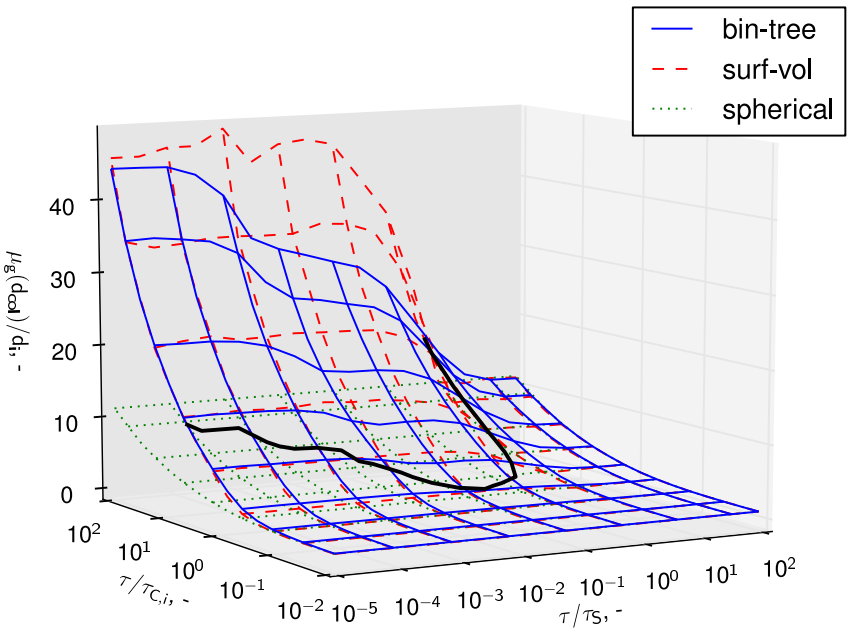

Figure 2: *Comparison of the normalised geometric mean collision diameter as a function of dimensionless coagulation and sintering time for each of the three particle models. The thick line depicts the intersection of the binary tree and surface-volume model predictions.*

of particles where only coagulation and sintering could operate at a specified rate.

The results of this analysis are presented in Figure 2, where the collision diameter (normalised by initial particle diameter) is plotted against the dimensionless sintering and initial coagulation time. The collision diameter was chosen as it is a strong function of type-space and is a good descriptor of overall aggregate size.

It is unsurprising that the models converge for high values of τ/τ_S. This corresponds to instantaneous sintering (or coalescence) of particles upon collision. It is interesting to observe that for some combinations of $(\tau/\tau_S, \tau/\tau_{C,i})$ the particles obtained through the binary tree model are larger; whereas for other combinations they appear smaller than the surface-volume model. Indeed, an intersection between these surfaces defines a line at which the particles obtained through both models are identical. This is shown in more detail in Figure 3, where the contours corresponding to the intersection of the binary tree and surface-volume models, and $\pm 5\%$ relative difference between the two are plotted.

Three zones in this figure are identified, corresponding to different 'types' of particles. Particles obtained in the spherical zone sinter sufficiently quickly to coalesce into spherical particles. In this zone, the all particle models effectively reduce to the spherical

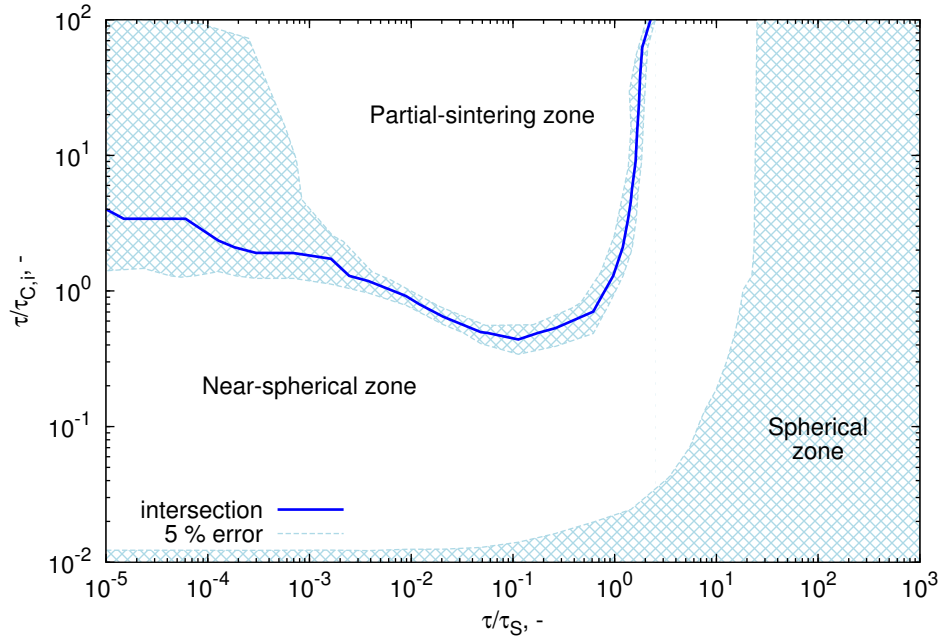

Figure 3: *A contour plot depicting where the binary tree model is equivalent to the surface-volume model. The shading corresponds to within 5% deviation (with respect to collision diameter) of the surface-volume model from the binary tree model.*

particle model; and there is no benefit gained from tracking the additional structural detail of particles.

In the near-spherical zone, aggregates containing few primary particles are formed, either due to a fast sintering rate or a slow coagulation rate. Figure 2 illustrates that the particles predicted by the binary tree model have a larger collision diameter, corresponding to smaller primary particles. The reason for this can be understood by considering the derived properties of the particle models, in particular the expressions for collision diameter. It is shown in the Appendix that, for coagulation of similarly-sized particles, the surface-volume model will under-estimate the predictions of the binary-tree model to a maximum of 10% difference. While this deviation is small, it causes potentially large changes in the rate of coagulation (rate $\propto d_{\mathrm{col}}^2$ in the free-molecular regime), thus increasing the maximum error.

In the partial-sintering zone, particles coagulate to form partially-sintered aggregates with more than 2–3 primary particles. Here, the surface-volume model over-predicts the results of the binary tree model. The reason for this can be understood by considering the sinterable surface area of an aggregate. As each connection node in the binary tree model is individually sintered (according to Equation (17)) there must always be more sinterable surface area in an aggregate described by the binary tree model than one described by the surface-volume model. Thus, aggregates will sinter faster, leading to the binary tree model predicting smaller aggregates with larger primaries.

The intersection of the partial-sintering and near-spherical zones corresponds to the point

where primaries are uniformly sized within an aggregate. As $\tau/\tau_S \to 0$ the binary tree model becomes the identical to the surface-volume model: aggregates are composed of un-sintered monodisperse primary particles.

3.2 Effect of polydispersity

The study in the previous section highlighted that under certain conditions, the surface-volume model yields aggregate particles with approximately the same size as the binary tree model. This, however, was determined for an initially monodisperse ensemble of particles (initial geometric standard deviation $\sigma_g(d_i) = 1.0$). The purpose of this case study is to investigate how polydispersity can affect model performance, under conditions where the surface-volume and binary-tree models are equivalent for monodisperse particles. To investigate this, a point on the intersection line of Figure 3 was chosen ($\tau/\tau_S = 1.4$, $\tau/\tau_{C,i} = 5.0$) and ensembles initialised with spherical particles of increasing polydispersity (up to $\sigma_g(d_i) = 3.0$). The results are given in Figure 4.

It is evident that the the surface-volume and binary-tree models perform comparably with $\sigma_g(d_i) < 1.5$. Under these conditions, there appears to be good agreement with the geometric mean collision and primary diameter and a small difference in geometric standard deviation of both. Beyond $\sigma_g(d_i) = 1.5$, the binary-tree model appears to predict larger aggregates with smaller primaries than the surface-volume model. This is attributed to the phenomenon discussed in Section 3.1 for the prediction of collision diameter in the near-spherical zone.

It is also interesting to observe that for the binary tree model, the standard deviation of the average primary diameter is significantly smaller than the average standard deviation of the primary diameter. This suggests that the local polydispersity within a particle can often be quite different to the polydispersity of the ensemble. The right panels of Figure 4 show that the spherical particle model yields ensembles with $\sigma_g(d) \approx 1.4$ for $\sigma_g(d_i) > 1.5$. This indicates that the system has reached the self-preserving particle size distribution [42].

In summary, this case study demonstrates that the prediction of the properties of an ensemble of polydisperse particles undergoing coagulation and is strongly dependent on choice of particle model. Highly polydisperse $\sigma_g(d_i) > 1.5$ systems are poorly described by the spherical or surface-volume models where coagulation and sintering occur on similar timescales.

4 Application to model systems

The case studies presented in the previous section were based on initialised ensembles of particles which could only undergo coagulation and sintering. However, in practical modelling applications, terms for inception, surface reaction and condensation are also often included. This section presents two models in which quite different particle structures are obtained. For both studies, the characteristic coagulation time is estimated using the

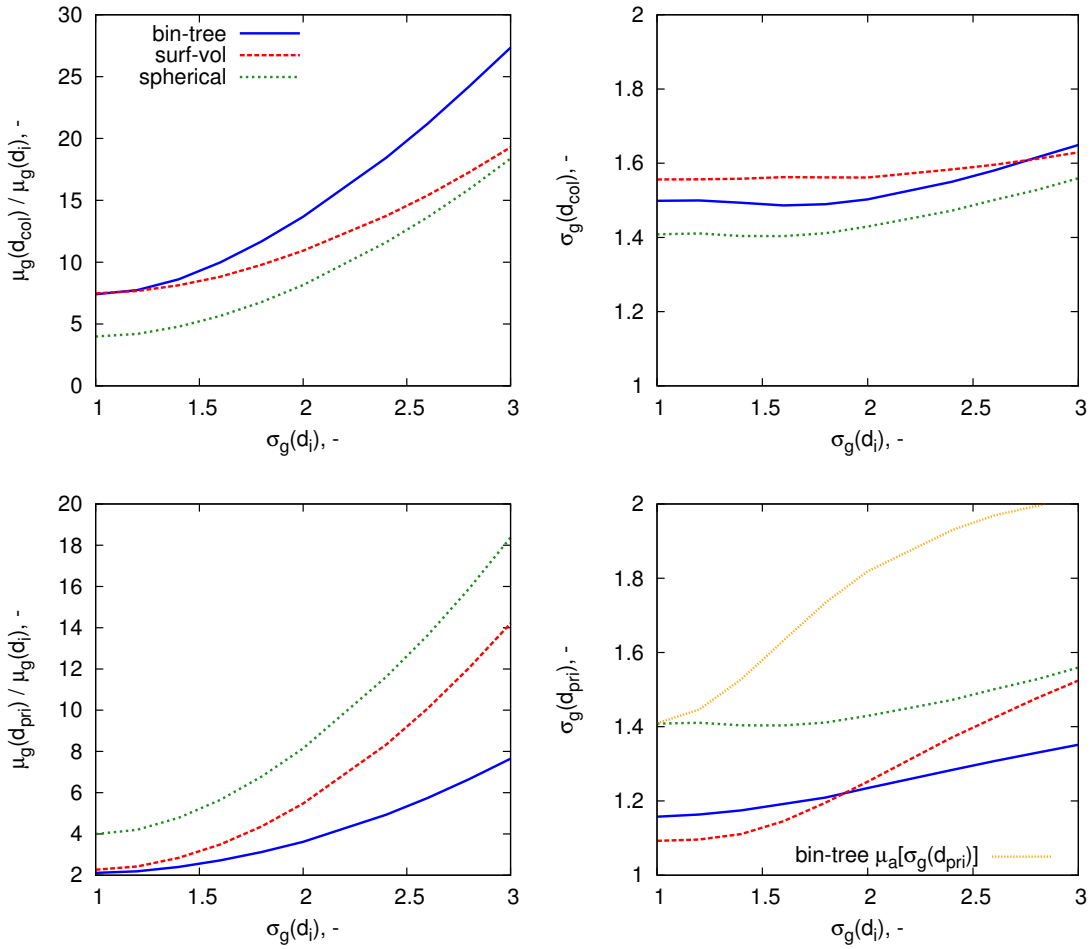

Figure 4: *Effect of initial polydispersity, $\sigma_g(d_i)$, on morphology of particles. Shown are the normalised geometric mean μ_g and standard deviation σ_g of the collision and primary diameter. These were generated for $\tau/\tau_S = 1.4$, $\tau/\tau_{C,i} = 5.0$, on the 'intersection' line of Figure 3.*

average properties of the ensemble:

$$\tau_{\mathrm{C}}(t) = \frac{1}{M_0(t) K^{\mathrm{tr}}\left(\mu_{\mathrm{a}}\left[d_{\mathrm{col}}\right](t), \mu_{\mathrm{a}}\left[m\right](t)\right)} \tag{23}$$

The expressions commonly-encountered for the characteristic sintering time are highly non-linear in diameter and temperature [4, 16, 24, 37]. Thus, the three particle models will begin to diverge when sintering moves from effectively instantaneous (very small particles) to finite-rate. The maximum primary particle diameter is therefore used to calculate the representative sintering time of the ensemble:

$$\tau_{\mathrm{S}}(t) = \tau_{\mathrm{S}}\left(\max\left[d_{\mathrm{pri}}\right](t), T(t)\right) \tag{24}$$

4.1 Silica model

An adaptation of the binary-tree model to silica was presented by Shekar et al. [39]. It has been used in a well-documented test case, in which the decomposition of 250 ppm tetraethoxysilane (TEOS) in N_2 at a constant temperature of 900°C at 1 atm is investigated [23, 39]. It is worthy of note that this model includes expressions for heterogeneous surface growth and intra-particle reactions. In particular, the sintering time is given by an expression obtained through model-fitting [37]:

$$\tau_S = A_S d_{pri} \exp\left(\frac{E_S}{T}\left[1 - \frac{d_{p,min}}{d_{pri}}\right]\right) \tag{25}$$

where, like A_S and E_S; $d_{p,min}$ is another empirical constant (Table 1). Adapting the expressions in [38] to the type-space of the surface-volume and spherical particle models, the temporal evolution of ensemble and particle characteristics are given in Figure 5.

Unsurprisingly, the spherical particle model performs poorly. This is to be expected given that the particles formed in this test system are aggregates. The surface-volume model is accurately able to capture the geometric standard deviation of the average estimated primary diameter $\sigma_g(\overline{d_{pri}})$. This is attributed to the *physical narrowing* of the primary particle size distribution due to sintering, as observed by Heine and Pratsinis [12]. The 'spike' in geometric standard deviation in the major particle growth phase is due to simultaneous inception and coagulation and is consistent with previous modelling studies [12].

As noted in Section 3.2, it is possible that the use of $\sigma_g(\overline{d_{pri}})$ across the particle ensemble may not fully capture the polydispersity of primaries in the aggregate. The slow increase of $\mu_a[\sigma_g(d_{pri})]$ as opposed to the 'spike' in $\sigma_g(\overline{d_{pri}})$ indicates that the perceived polydispersity of the ensemble is quite different to that within an aggregate particle. This is potentially important structural information which can not be resolved from surface-volume or spherical particle models.

The map of model performance as a function of amount of coagulation and sintering (Figure 3) is a useful tool in understanding where and why models begin to differ. It can also be applied to these specific modelling examples. As such, the movement of the particle ensemble with time t through the t/τ_C, t/τ_S space is plotted in Figure 6.

The very small values obtained for t/τ_S are associated with the strong diameter dependence in Equation (25). The near-spherical zone was therefore extrapolated from $t/\tau_S = 10^{-5}$ to account for this. The rapid movement across the space (as shown by the labelled times) is attributed to the fast growth of particles due to simultaneous surface reaction, coagulation and sintering.

At early times, particles are spherical and in high number concentration. This causes the system to start in the 'spherical zone', at high values of t/τ_S. As particles grow, their characteristic sintering time increases. This causes a shift to lower values of t/τ_S. At the same time, the rate of coagulation slowly decreases, primarily due to the decrease in number density M_0. Finally, as the primary particle distribution becomes physically narrowed by sintering, the primary diameter ceases to change with time (Figure 5), allowing t/τ_S to steadily increase with increasing time t.

The models effectively separate paths once coagulation begins. This is evident in Figures

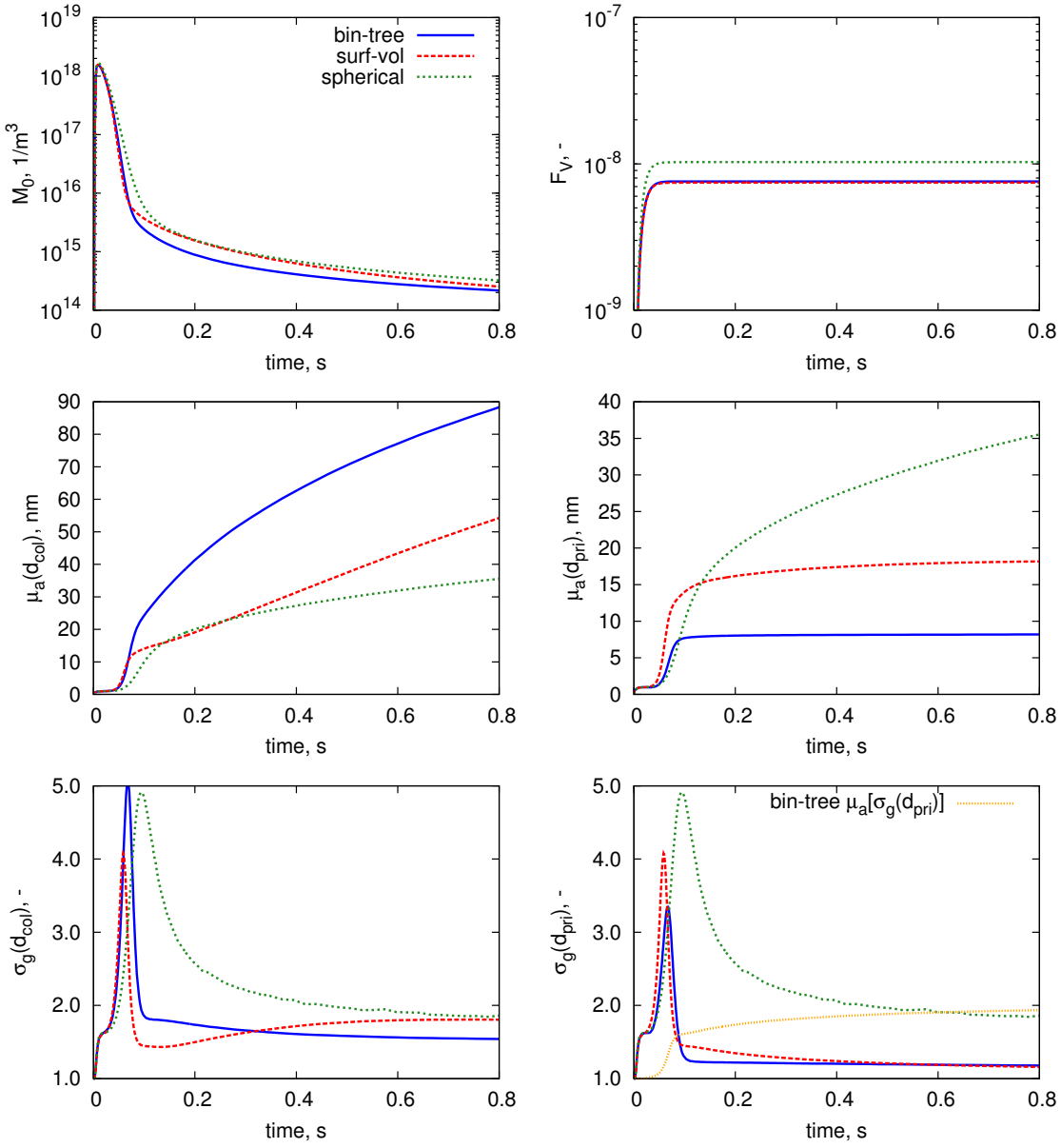

Figure 5: *Comparison of model predictions for the silica system of Shekar et al. [38]. Depicted are the zeroth moment (M_0), volume fraction (F_V), arithmetic mean (μ_a) and geometric standard deviation (σ_g) of the collision and primary diameters.*

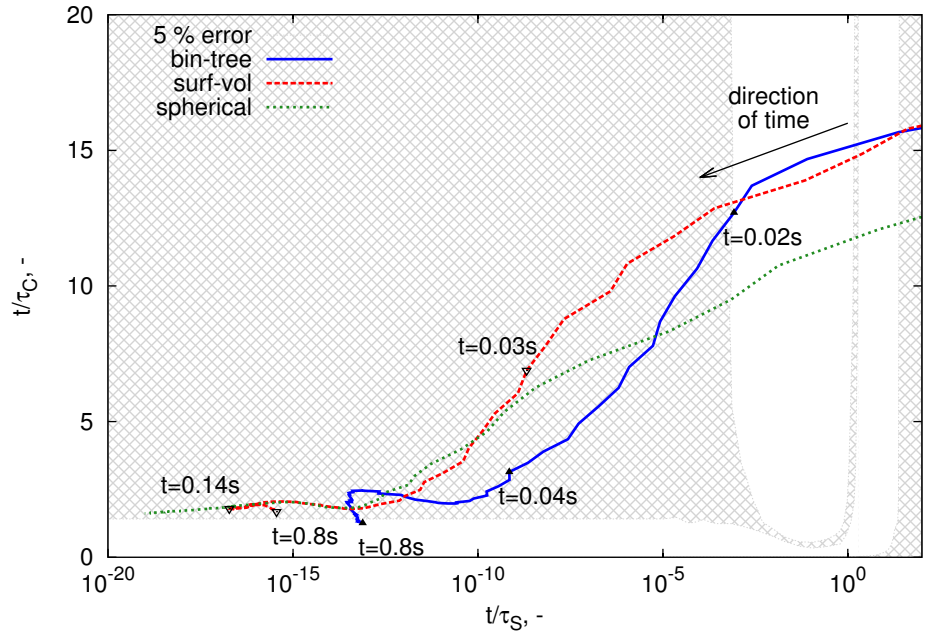

Figure 6: *Trajectory of the case of Shekar et al. [39] through the t/τ_C, t/τ_S space. The shading depicts the 5% error margins as described in Figure 3. Specific process times for the binary-tree and surface-volume models from Figure 5 are labelled.*

5 and in Figure 6, soon after the trajectories exit the spherical zone. Figure 6 also illustrates that even a very small amount of time spent in the near-spherical or partial-sintering zone can cause the predictions of surface-volume model to markedly deviate from those of the binary-tree model.

4.2 Silicon model

The previous application focused on synthesis of aggregate particles, where coagulation and sintering are occurring on different timescales. It is, however, also common to attempt to model spherical or near-spherical particles [2, 18, 44], where these two key processes can operate on similar timescales. An example of these conditions was recently identified in a multivariate model for silicon nanoparticle synthesis [22], where silicon particles were manufactured in a hot wall reactor at atmospheric pressure [44].

In this model, a grain-boundary diffusion sintering kinetic [16, 20] is utilised with parameters given in Table 1. Terms for homogeneous nucleation, condensation, surface reaction and release of hydrogen are also included [22]. The evolution of important particle and ensemble characteristics for this model as applied to the case of Wu et al. [44] is given in Figure 7. Note that a temperature profile (increasing from 500°C to 1250°C) is imposed across this simulation [22, 26, 44].

In this case, all models predict that spherical particles are obtained at the end of the process time. However, neither the surface-volume nor the spherical particle model perform

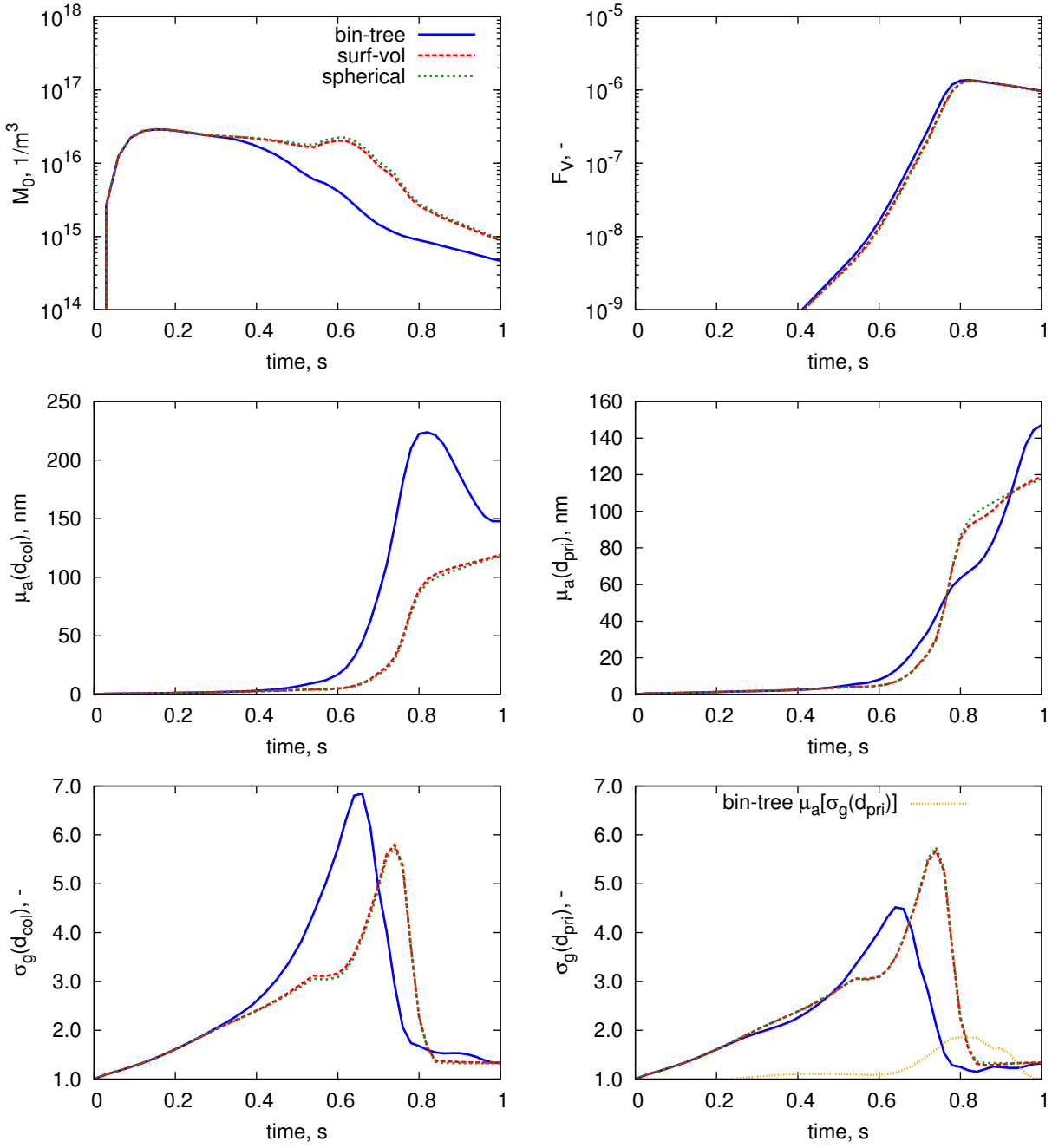

Figure 7: *Comparison of model predictions for the case of Wu et al. [44] using a multivariate silicon model [22]. Depicted are the zeroth moment (M_0), volume fraction (F_V), arithmetic mean (μ_a) and geometric standard deviation (σ_g) of the collision and primary diameters.*

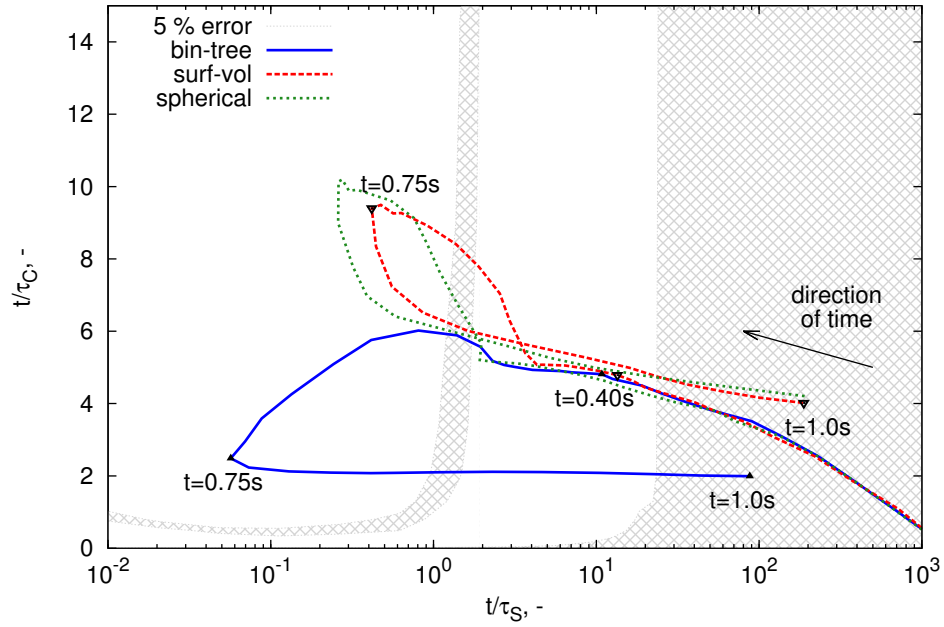

Figure 8: *Trajectory of the case of Wu et al. [44] using a multivariate silicon model [22] through the t/τ_C, t/τ_S space. The shading depicts the 5% error margins as described in Figure 3. Specific process times for the binary-tree and surface-volume models from Figure 7 are labelled, $t < 0.2$s omitted for clarity.*

comparably to the binary-tree model, with the number density M_0 double and average collision diameter $\mu_a(d_{col})$ 20 % lower than that of the binary-tree model's prediction. The surface-volume and spherical models predict the occurrence of a secondary nucleation period (at $t = 0.6$s in M_0 panel of Figure 8), consistent with other spherical particle modelling efforts [26] of this system.

The predictions of the surface-volume model are also very similar to those of the spherical particle model, despite containing a finite sintering rate. It is hypothesised that this is due to the high polydispersity of particles ($\sigma_g > 3.0$, Figure 7 lower panels) for this case study, resulting in a similar 'convergence' of the two models as depicted in Figure 4. To further understand the differences between models here, this case is plotted atop Figure 3's coagulation-sintering map in Figure 8.

Again, the system begins with small spherical particles at high t/τ_S. The three models diverge from each other after passing through the near-spherical zone. The surface-volume and spherical models subsequently show a large increase in coagulation rate, while it steadily decreases for the binary-tree model. This is due to the secondary nucleation period causing the number density to remain steady (Figure 7).

The minimum sintering rate reached at approximately 0.75 s represents the point at which the rate of decrease in sintering time is balanced by the contributions from the rate of increase in particle diameter and rate of increase in temperature. Past this point, the increasing temperature profile causes coalescence of aggregate structures, causing all models to return to the spherical zone. This case study highlights an example where experimental

insight should be used with caution: if spherical particles are obtained experimentally, it does not necessarily justify the use of a spherical particle model.

5 Conclusions

This work has presented the mathematical formulation of particle models commonly used in aerosol dynamics of nanoparticles. A detailed numerical study was conducted in order to understand under which conditions these models differ. Starting from a set of identical conditions, the predictions of the resulting average properties of the particle ensemble were compared for each of the particle models. It was identified that under certain circumstances, all models were equivalent to a spherical particle model.

Outside of this range, the performance of the popular and computationally inexpensive surface-volume model with respect to a model which tracks full aggregate structure (binary-tree model) was evaluated. The two models gave alike results (to within a small error margin) where sintering was slow. However, where coagulation and sintering occurred on a similar timescale, the models predicted substantially different results. Further, the spherical and surface-volume particle models were shown to incur a large error margin where the coagulating ensemble was highly polydisperse.

The three models were also applied to modelling systems presented in earlier work. The first investigated aggregate formation where sintering primarily occurs on a much slower timescale than coagulation. Secondly, a model of silicon nanoparticle synthesis in which coagulation and sintering occur on approximately equal timescales was investigated. Here, it was evident that the additional structural information of the binary-tree model is essential in capturing the polydispersity of the ensemble and finite sintering kinetics of particles.

There is still considerable scope for further investigation of the behaviour of particle models. Heterogeneous growth processes are well-documented contributors to rounding of particles [21, 39] and have not been explicitly addressed in the present work. Further, only the most popular version of the surface-volume model has been used, when alternative two-dimensional formulations [12, 27] and different expressions for derived properties [43] exist.

As many population balance models use some degree of fitting or parameter estimation [6, 24, 37], the error in use of a 'simple' model will be reflected in the parameters obtained through the fitting procedure. The present work highlights that the choice of particle model *does* matter, and that a target modelling system should be well-characterised experimentally before proceeding to modelling.

6 Acknowledgements

W.J.M. acknowledges funding from the Cambridge Australia Trust to undertake this work. The authors additionally wish to thank the members of the Computational Modelling

Group for their guidance and support. M.K. gratefully acknowledges the DFG Mercator programme and the support of CENIDE at the Unviversity of Duisburg Essen.

A Collisions in the near-spherical zone

Suppose two spherical particles with volume v_1 and kv_1 collide. How do the derived properties of the resulting particles differ? The total surface are of the resulting particle is given by

$$S = \pi \left(\frac{6v_1}{\pi}\right)^{\frac{2}{3}} \left[1 + k^{\frac{2}{3}}\right] \ . \tag{A.1}$$

The equivalent spherical diameter is given by

$$d_{\text{sph}} = \left(\frac{6v_1}{\pi}\right)^{\frac{1}{3}} \left[1 + k\right]^{\frac{1}{3}} \ . \tag{A.2}$$

Thus, the collision diameter as predicted by the surface-volume model may be calculated:

$$d_{\text{col}}^{\text{surf-vol}} = \frac{1}{2} \left(\frac{6v_1}{\pi}\right)^{\frac{1}{3}} \left[(1+k)^{\frac{1}{3}} + \sqrt{1 + k^{\frac{2}{3}}}\right] \tag{A.3}$$

The binary-tree model requires estimation of the average primary diameter

$$\overline{d_{\text{pri}}} = \frac{1}{2} \left(\frac{6v_1}{\pi}\right)^{\frac{1}{3}} \left[1 + k^{\frac{1}{3}}\right] \tag{A.4}$$

Using this information, and calculating the 'reduced number of primary particles' (given by the term inside the $\frac{1}{D_{\text{f}}}$ exponent) the binary-tree model calculates the collision diameter of the aggregate particle as

$$d_{\text{col}}^{\text{bin-tree}} = \frac{1}{2} \left(\frac{6v_1}{\pi}\right)^{\frac{1}{3}} \left[1 + k^{\frac{1}{3}}\right] \left(\frac{\left[1 + k^{\frac{2}{3}}\right]^3}{\left[1+k\right]^2}\right)^{\frac{1}{D_{\text{f}}}} \tag{A.5}$$

The two models are compared by plotting the ratio of $d_{\text{col}}^{\text{bin-tree}}$ to $d_{\text{col}}^{\text{surf-vol}}$ using a fractal dimension $D_{\text{f}} = 1.8$ and $D_{\text{f}} = 1.56$. It is evident that for like-sized particles ($k \approx 1$) the collision diameter as predicted by the surface-volume model will be smaller than that predicted by the binary-tree particle model to a maximum of 10% under-estimation.

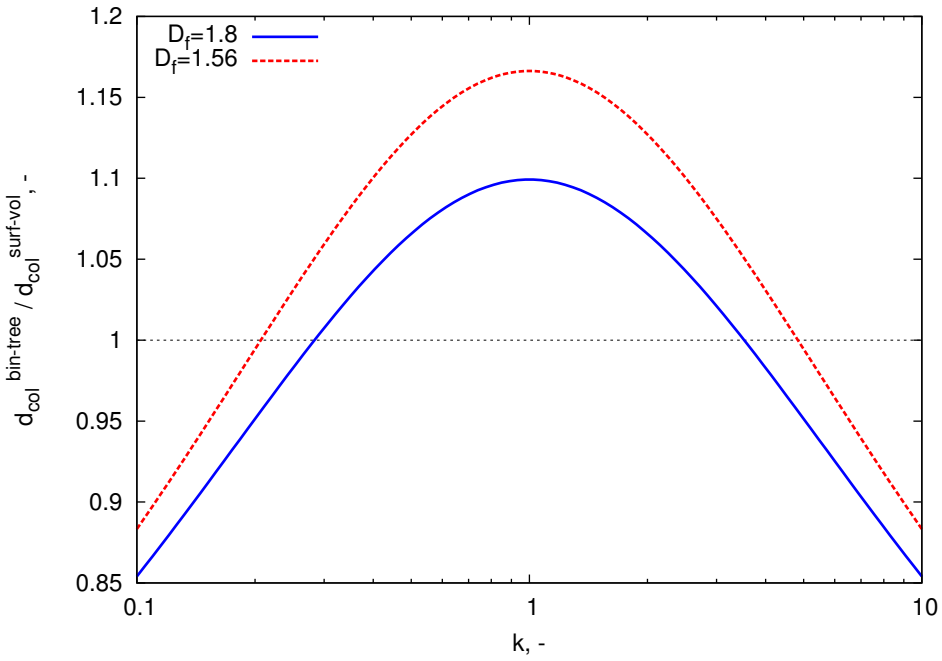

Figure A.1: *Ratio of collision diameters predicted for the surface-volume and binary tree models as a function of relative colliding particle size.*

References

[1] J. Akroyd, A. Smith, R. Shirley, L. McGlashan, and M. Kraft. A coupled CFD-population balance approach for nanoparticle synthesis in turbulent reacting flows. *Chemical Engineering Science*, 66(17):3792–3805, 2011.

[2] U. Backman, J. Jokiniemi, A. Auvinen, and K. Lehtinen. The effect of boundary conditions on gas-phase synthesised silver nanoparticles. *Journal of Nanoparticle Research*, 4(4):325–335, 2002.

[3] M. Balthasar and M. Kraft. A stochastic approach to calculate the particle size distribution function of soot particles in laminar premixed flames. *Combustion and Flame*, 133(3):289–298, 2003.

[4] B. Buesser, A. Gröhn, and S. Pratsinis. Sintering rate and mechanism of TiO_2 nanoparticles by molecular dynamics. *The Journal of Physical Chemistry C*, 115 (22):11030–11035, 2011.

[5] M. Celnik, R. Patterson, M. Kraft, and W. Wagner. Coupling a stochastic soot population balance to gas-phase chemistry using operator splitting. *Combustion and Flame*, 148(3):158–176, 2007.

[6] D. Chen, Z. Zainuddin, E. Yapp, J. Akroyd, S. Mosbach, and M. Kraft. A fully coupled simulation of PAH and soot growth with a population balance model. *Proceedings of the Combustion Institute*, In press.

[7] M. Eggersdorfer, D. Kadau, H. Herrmann, and S. Pratsinis. Aggregate morphology evolution by sintering: Number & diameter of primary particles. *Journal of Aerosol Science*, 46:7–19, 2012.

[8] M. Frenklach. Method of moments with interpolative closure. *Chemical Engineering Science*, 57(12):2229–2239, 2002.

[9] M. Frenklach and S. Harris. Aerosol dynamics modeling using the method of moments. *Journal of colloid and interface science*, 118(1):252–261, 1987.

[10] M. Goodson and M. Kraft. An efficient stochastic algorithm for simulating nanoparticle dynamics. *Journal of Computational Physics*, 183(1):210–232, 2002.

[11] M. Gröschel, R. Körmer, M. Walther, G. Leugering, and W. Peukert. Process control strategies for the gas phase synthesis of silicon nanoparticles. *Chemical Engineering Science*, 73:181–194, 2012.

[12] M. Heine and S. Pratsinis. Polydispersity of primary particles in agglomerates made by coagulation and sintering. *Journal of aerosol science*, 38(1):17–38, 2007.

[13] P. Ho, M. Coltrin, and W. Breiland. Laser-induced fluorescence measurements and kinetic analysis of Si atom formation in a rotating disk chemical vapor deposition reactor. *The Journal of Physical Chemistry*, 98(40):10138–10147, 1994.

[14] M. Hounslow. A discretized population balance for continuous systems at steady state. *AIChE Journal*, 36(1):106–116, 1990.

[15] A. Kazakov and M. Frenklach. Dynamic modeling of soot particle coagulation and aggregation: Implementation with the method of moments and application to high-pressure laminar premixed flames. *Combustion and Flame*, 114(3):484–501, 1998.

[16] A. Kobata, K. Kusakabe, and S. Morooka. Growth and transformation of TiO_2 crystallites in aerosol reactor. *AIChE journal*, 37(3):347–359, 1991.

[17] W. Koch and S. Friedlander. The effect of particle coalescence on the surface area of a coagulating aerosol. *Journal of Colloid and Interface Science*, 140(2):419–427, 1990.

[18] R. Körmer, H. Schmid, and W. Peukert. Aerosol synthesis of silicon nanoparticles with narrow size distribution–Part 2: Theoretical analysis of the formation mechanism. *Journal of Aerosol Science*, 41(11):1008–1019, 2010.

[19] M. Kraft. Modelling of particulate processes. *Kona, Powder and Particle*, 23:18–35, 2005.

[20] F. Kruis, K. Kusters, S. Pratsinis, and B. Scarlett. A simple model for the evolution of the characteristics of aggregate particles undergoing coagulation and sintering. *Aerosol Science and Technology*, 19:514–526, 1993.

[21] P. Lavvas, M. Sander, M. Kraft, and H. Imanaka. Surface chemistry and particle shape: Processes for the evolution of aerosols in titan's atmosphere. *The Astrophysical Journal*, 728(2):80, 2011.

[22] W. Menz and M. Kraft. A new model for silicon nanoparticle synthesis. *Combustion & Flame*, (accepted for publication).

[23] W. Menz, R. Patterson, W. Wagner, and M. Kraft. Application of stochastic weighted algorithms to a multidimensional silica particle model. *Journal of Computational Physics*, (submitted for review).

[24] W. Menz, S. Shekar, G. Brownbridge, S. Mosbach, R. Körmer, W. Peukert, and M. Kraft. Synthesis of silicon nanoparticles with a narrow size distribution: a theoretical study. *Journal of Aerosol Science*, 44:46–61, 2012.

[25] N. Morgan, C. Wells, M. Goodson, M. Kraft, and W. Wagner. A new numerical approach for the simulation of the growth of inorganic nanoparticles. *Journal of Computational Physics*, 211(2):638–658, 2006.

[26] H. Nguyen and R. Flagan. Particle formation and growth in single-stage aerosol reactors. *Langmuir*, 7(8):1807–1814, 1991.

[27] S. Park and S. Rogak. A novel fixed-sectional model for the formation and growth of aerosol agglomerates. *Journal of Aerosol Science*, 35(11):1385–1404, 2004.

[28] R. Patterson and M. Kraft. Models for the aggregate structure of soot particles. *Combustion and Flame*, 151(1-2):160–172, 2007.

[29] R. Patterson and W. Wagner. A stochastic weighted particle method for coagulation–advection problems. *SIAM Journal on Scientific Computing*, 34(3):290–311, 2012.

[30] R. Patterson, J. Singh, M. Balthasar, M. Kraft, and W. Wagner. Extending stochastic soot simulation to higher pressures. *Combustion and Flame*, 145(3):638–642, 2006.

[31] R. Patterson, W. Wagner, and M. Kraft. Stochastic weighted particle methods for population balance equations. *Journal of Computational Physics*, 230:7456–7472, 2011.

[32] S. Rogak, R. Flagan, and H. Nguyen. The mobility and structure of aerosol agglomerates. *Aerosol Science and Technology*, 18(1):25–47, 1993.

[33] M. Sander, R. West, M. Celnik, and M. Kraft. A detailed model for the sintering of polydispersed nanoparticle agglomerates. *Aerosol Science and Technology*, 43(10): 978–989, 2009.

[34] M. Sander, R. Patterson, A. Braumann, A. Raj, and M. Kraft. Developing the PAH-PP soot particle model using process informatics and uncertainty propagation. *Proceedings of the Combustion Institute*, 33(1):675–683, 2011.

[35] D. Schaefer and A. Hurd. Growth and structure of combustion aerosols: fumed silica. *Aerosol Science and Technology*, 12(4):876–890, 1990.

[36] H. Schmid, S. Tejwani, C. Artelt, and W. Peukert. Monte carlo simulation of aggregate morphology for simultaneous coagulation and sintering. *Journal of Nanoparticle Research*, 6(6):613–626, 2004.

[37] S. Shekar, M. Sander, R. Riehl, A. Smith, A. Braumann, and M. Kraft. Modelling the flame synthesis of silica nanoparticles from tetraethoxysilane. *Chemical Engineering Science*, 70:54–66, 2011.

[38] S. Shekar, W. Menz, A. Smith, M. Kraft, and W. Wagner. On a multivariate population balance model to describe the structure and composition of silica nanoparticles. *Computers & Chemical Engineering*, 43:130–147, 2012.

[39] S. Shekar, A. Smith, W. Menz, M. Sander, and M. Kraft. A multidimensional population balance model to describe the aerosol synthesis of silica nanoparticles. *Journal of Aerosol Science*, 44:83–98, 2012.

[40] S. Tsantilis and S. Pratsinis. Evolution of primary and aggregate particle-size distributions by coagulation and sintering. *AIChE Journal*, 46(2):407–415, 2000.

[41] S. Tsantilis, H. Kammler, and S. Pratsinis. Population balance modeling of flame synthesis of titania nanoparticles. *Chemical Engineering Science*, 57(12):2139–2156, 2002.

[42] S. Vemury and S. Pratsinis. Self-preserving size distributions of agglomerates. *Journal of Aerosol Science*, 26(2):175–185, 1995.

[43] C. Wells, N. Morgan, M. Kraft, and W. Wagner. A new method for calculating the diameters of partially-sintered nanoparticles and its effect on simulated particle properties. *Chemical Engineering Science*, 61(1):158–166, 2006.

[44] J. Wu, H. Nguyen, and R. Flagan. A method for the synthesis of submicron particles. *Langmuir*, 3(2):266–271, 1987.

[45] Y. Xiong and S. Pratsinis. Formation of agglomerate particles by coagulation and sintering–Part I. A two-dimensional solution of the population balance equation. *Journal of Aerosol Science*, 24(3):283–300, 1993.

[46] H. Zhao and C. Zheng. A new event-driven constant-volume method for solution of the time evolution of particle size distribution. *Journal of Computational Physics*, 228(5):1412–1428, 2009.